Sensors and Actuators B 160 (2011) 1468–1472

Contents lists available at ScienceDirect

Sensors and Actuators B: Chemical

journal homepage: www.elsevier.com/locate/snb

Short communication

Highly sensitive SnO_2 hollow nanofiber-based NO_2 gas sensors

Nam Gyu Cho[a], Dae Jin Yang[b], Mi-Jin Jin[c], Ho-Gi Kim[a], Harry L. Tuller[b], Il-Doo Kim[a,*]

[a] Department of Materials Science and Engineering, Korea Advanced Institute of Science and Technology, Daejeon 305-701, Republic of Korea
[b] Department of Materials Science and Engineering, Massachusetts Institute of Technology, Cambridge, MA 02139, USA
[c] Optoelectronic Materials Center, Korea Institute of Science and Technology, P.O. Box 131 Cheongryang, Seoul 130-650, Republic of Korea

ARTICLE INFO

Article history:
Received 15 April 2011
Received in revised form 29 June 2011
Accepted 18 July 2011
Available online 23 July 2011

Keywords:
Tin oxide
Gas sensor
Electrospinning
Hollow
Nanofiber

ABSTRACT

SnO_2 hollow nanofibers (HNFs) with diameters of 300–500 nm were fabricated via electrospinning of templating nanofibers and RF-sputtering of SnO_2 thin overlayers (15–20 nm thick and comparable grain size) followed by heat-treatment at 450 °C. Gas sensors using these HNFs exhibited *n*-type gas sensing characteristics and an enhanced gas response to 2 ppm NO_2 (R_{gas}/R_{air} = 81.4) as compared to that (R_{gas}/R_{air} = 19.9) of planar SnO_2 thin films. The enhanced response to NO_2 is attributed to the greater accessible active area and the greater space charge modulation depth associated with the hollow thin walled structures.

1. Introduction

Metal oxide nanostructures such as nanofibers, nanorods, nanotubes and nanobelts have received considerable attention owing to their unique properties relative to bulk counterparts, especially for application to gas sensors, batteries, solar cells and other nanoelectronics [1,2]. Among these items, gas sensors, also known as chemiresistors, show considerable promise in environmental monitoring, the food industry and in areas related to domestic safety and security. Nanostructured metal oxides have high surface-to-volume ratios and reduced cross-sections, offering more effective modulation of resistivity by the gases, thereby leading to enhanced response and faster response/recovery speeds [3]. This is particularly true for metal oxide gas sensors utilizing well-aligned and gas accessible nanoporous structures which simultaneously offer compatibility with microelectronic fabrication processes [3,4]. Hierarchical and hollow structured micro/nano-sized materials are especially attractive for applications in chemical sensors [5]. These nano-building blocks provide enhanced surface activity, i.e., high surface reactions and fast diffusion, based on their low-density and high surface permeability, allowing easy gas penetration into the sensing layers [6–8].

The synthetic routes used for the fabrication of nanostructured metal oxides include physical deposition (vapor–solid/vapor–liquid–solid/solution–liquid–solid growth), thermal oxidation growth, hydrothermal/solvothermal method, and electrospinning [9,10]. Templating approaches using sacrificial layers, such as colloidal microspheres or electrospun polymeric fibers [11–14], represent one of several simple and attractive synthetic routes for producing hollow metal oxide nanostructures. The authors recently reported that gas sensors using SnO_2 hollow hemispheres, synthesized with the aid of PMMA microsphere templates, exhibited an approximately 3-fold enhancement in NO_2 gas response compared to their non-templated counterparts [15]. Although the colloidal templating method successfully demonstrated improvements in gas response, the fabrication of large-scale templated films remains a challenge due to the difficulty in achieving a large homogeneous area with controlled film uniformity. On the other hand, electrospinning is a very simple and versatile approach for producing polymeric nanofiber templates with diameters down to tens of nanometers and lengths of up to several centimeters with controllable morphologies and large-scale production capability [10]. More recently, the authors synthesized hollow ZnO microtubes using electrospun nanofibers as templates and demonstrated that ZnO microtube based gas sensors showed four times higher sensitivities (depending on fiber configurations) compared to planar ZnO thin film sensors [16]. However, a major drawback of the previously investigated ZnO microtube sensors was their high base resistance (~0.15 MΩ), resulting in difficulties with signal acquisition. By reducing device resistance, while maintaining the unique nanoporous morphology, one can envision the operation of gas sensors at lower temperatures and more applicable ranges for many micro-scaled sensor devices.

* Corresponding author. Tel.: +82 42 350 3310; fax: +82 42 350 3329.
E-mail address: idkim@kaist.re.kr (I.-D. Kim).

0925-4005/$ – see front matter © 2011 Elsevier B.V. All rights reserved.
doi:10.1016/j.snb.2011.07.035

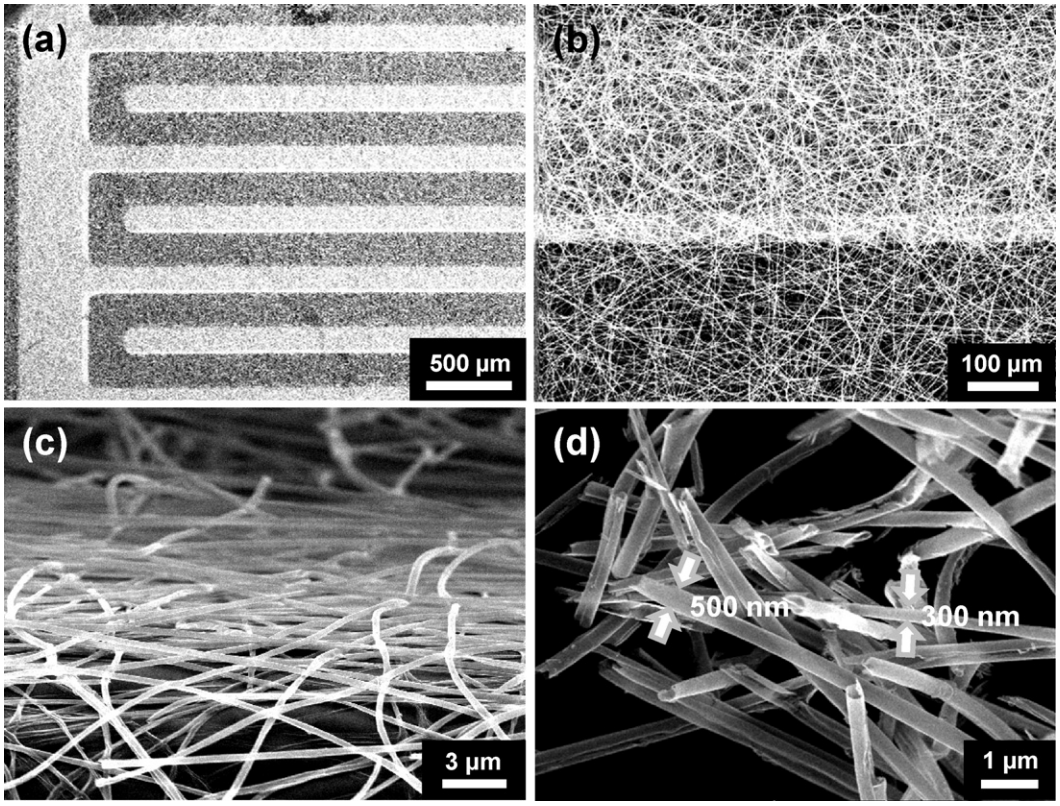

Fig. 1. SEM images of SnO_2 HNFs; (a) top view of interdigitated electrode; (b) plan view – intermediate magnification showing arrangement of HNFs; (c) tilt view – intermediate magnification showing randomly arrayed HNFs; (d) cross sectional view showing the SnO_2 nanofiber with pipe, cylindrical and hollow shapes.

In this work, we present the facile fabrication of low resistance SnO_2 hollow nanofibers (HNFs) via physical thin film growth on polymeric sacrificial template prepared by electrospinning, followed by subsequent heat-treatment. These types of HNFs, with very thin sensing layers of shell thickness of ~20 nm, are preferable given fast gas diffusion and high surface activity resulting from nearly full electron depletion of the shells. A gas sensor based on SnO_2 HNFs was tested and compared with a planar SnO_2 thin film in low-ppm-level nitrogen dioxide (NO_2) gases, important for monitoring environmental pollution resulting from combustion or automotive emissions.

2. Experimental

PVP-PMMA composite fibers were electrospun from a solution of N,N-dimethylformamide (DMF, Fluka, 98%), polymethylmethacrylate (PMMA), $M_w \approx 350{,}000$ g/mol, Aldrich) and poly(vinyl pyrrolidone) (PVP, $M_w \approx 1{,}300{,}000$ g/mol). The composite fibers were used as a sacrificial polymeric template. The PVP-PMMA, with a 50/50 weight ratio, dissolved in the DMF, was loaded into a plastic syringe with a stainless-steel needle of 0.25 mm (25GA) diameter. The precursor solution was pumped through the nozzle at a constant rate of 50 μL/min. A voltage of 20 kV was applied between the tip and the substrate, placed 15 cm below the needle tip to collect the PVP-PMMA fiber mats. SiO_2-coated silicon wafers, fitted with interdigitated electrodes (16 fingers, 8 mm long and 200 μm wide, spaced 200 μm apart) comprising 200 nm thick gold electrodes on a 50 nm thick titanium adhesion layer, were used as sensor substrates.

Following the electrospinning of the PVP-PMMA composite fiber templates, a 50 nm overlayer of SnO_2 was sputtered onto PVP-PMMA fiber mats. The mats in turn, covered the SiO_2 substrates with and without interdigitated Au electrode arrays (200 μm Au fingers spaced 200 μm apart). Reference specimens comprising SnO_2 thin films deposited directly onto interdigitated alumina substrates without the templates were also prepared. The SnO_2 layer was sputtered from a 3-in. SnO_2 target using an RF power of 70 W under a flow of Ar (20 sccm) at a working pressure of 1.33 Pa. The substrates were not heated during the sputtering process to prevent thermal decomposition of the as-spun PVP-PMMA fiber templates. The melting temperatures (T_m) of the PMMA and PVP were 160 °C and 180 °C, respectively. After the SnO_2 deposition, a post-annealing process was performed using a box furnace at 450 °C for 30 min in an air to remove the as-spun PVP-PMMA fiber templates and to crystallize the SnO_2 overlayers.

The morphology and microstructure of the SnO_2 HFs were analyzed using a field-effect scanning electron microscope (FE-SEM, Philips XL30SFEG) and a transmission electron microscope (TEM, Tecnai G2 F30 S-TWIN). The crystal structure of the SnO_2 HFs was characterized by an X-ray diffractometer (Rigaku D/MAX-IIIC using CuK_α radiation).

SnO_2 thin films and SnO_2 HNFs based sensors were prepared on Au interdigitated electrodes. Each SnO_2 (thin film and HNF) sensor was placed in a quartz tube chamber stabilized at a constant sensing temperature (300 °C). The gas concentration was controlled by changing the mixing ratio of the target gases and dry synthetic air. The gas sensing measurements were carried out by monitoring changes in the DC resistance of R_{gas}/R_{air} (R_{gas}: resistance during exposure to the target gas, R_{air}: resistance in air atmosphere) during cyclic exposure to trace concentrations (between 0.5 and 2 ppm) of NO_2 in dry air. A constant flow rate of 500 sccm (standard cubic centimeter per minute) was used to avoid possible variations in the sensing temperature upon exposure to the gas. The DC 2 probe resistance of the sensor was measured using a Digital Multi Meter (NI PXI-1042Q) interfaced with a computer.

3. Results and discussion

The diameter of the as-spun PVP-PMMA fibers ranged between 400 and 600 nm. After the growth of the SnO_2 overlayers onto the fiber templates, the SnO_2 shells uniformly covered the entire length of the PVP-PMMA composite fibers. Following calcination at 450 °C, the organic (PVP-PMMA) fiber cores decomposed, leaving only the inorganic (SnO_2) shells. As a result, SnO_2 HNFs, replicating the random structure of the as-spun PVP-PMMA fiber mats, were produced. Due to very thin wall thickness, higher calcination temperatures often resulted in the collapse of the tube structure. As a consequence, the SnO_2 overlayers were calcined at relatively low temperature (450 °C) in order to maintain the hollow shape of the sub-micron SnO_2 tubes. Fig. 1a and b shows SEM images of the SnO_2 HNF networks prepared on the sensor substrates. The SnO_2 HNF networks exhibit randomly oriented morphologies in the form of nonwoven mats with a fiber diameter range of 300–500 nm, as shown in Fig. 1b and c. Slight shrinkage was observed due to the densification of the SnO_2 shells following the decomposition of the PVP-PMMA polymers during the heat-treatment. The cross-sectional image of the SnO_2 fiber mats clearly exhibits the hollow structures (Fig. 1d). This unique morphology results in ready gas accessibility to the exceptionally high surface-to-volume ratio structure as compared to dense SnO_2 thin films.

The crystalline structure of the SnO_2 HNFs was examined by X-ray diffraction (XRD). Fig. 2 shows the XRD pattern of the SnO_2 HNFs after calcination at 450 °C for 30 min. The XRD spectra show that the SnO_2 hollow fiber mats crystallized into the rutile structure with primarily (1 1 0), (1 0 1), and (2 1 1) orientations. The crystallite sizes of the SnO_2 hollow fiber structure were calculated using Scherrer's equation ($D = 0.94\lambda/\beta\cos(2\theta)$, where D is the mean grain size, λ is the wavelength of the X-ray radiation ($\lambda = 0.154$ nm for

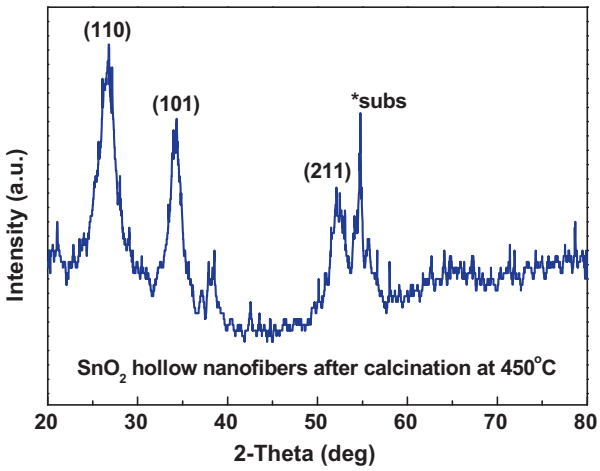

Fig. 2. XRD pattern for the calcined SnO_2 HNFs prepared on Si substrate.

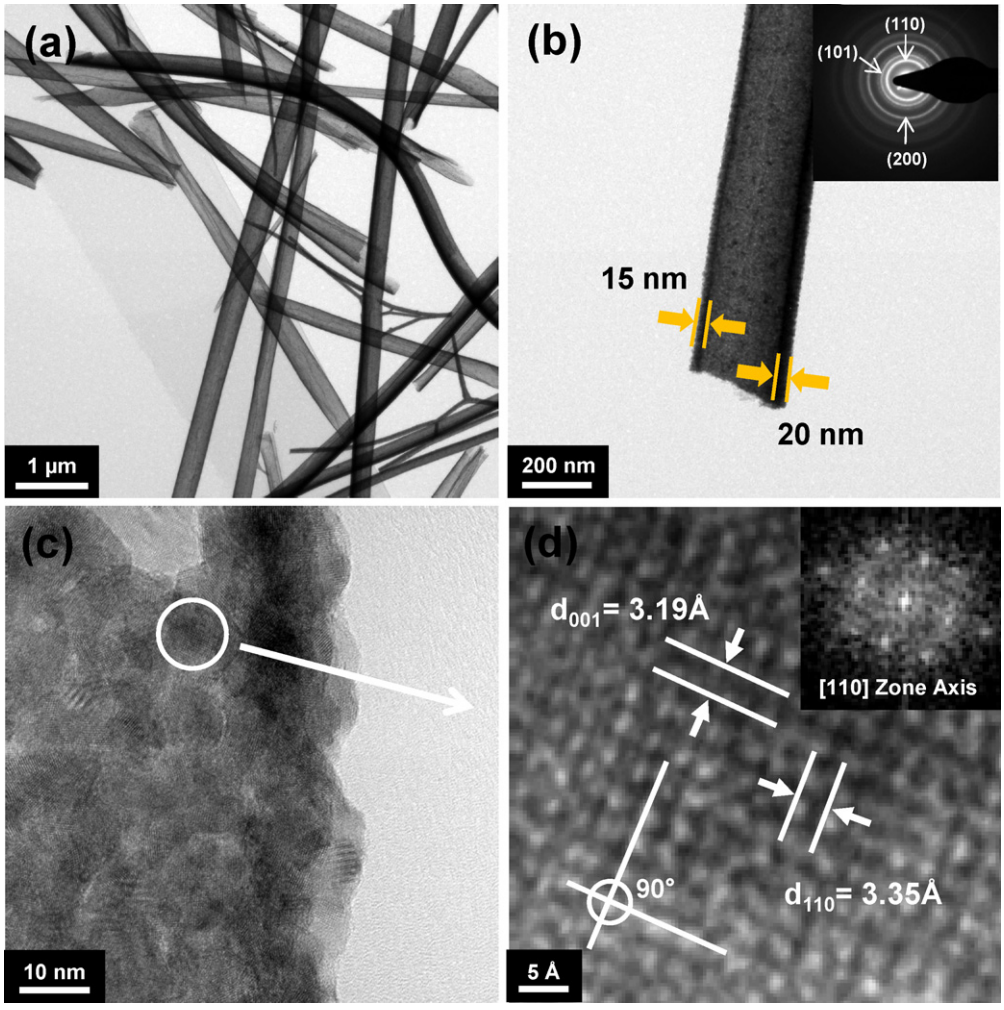

Fig. 3. (a) Low resolution TEM micrographs of SnO_2 HNFs, (b) and individual SnO_2 HNFs showing shell thickness, (c) HR image showing polycrystalline, (d) enlarged lattice image and corresponding FFT pattern (inset).

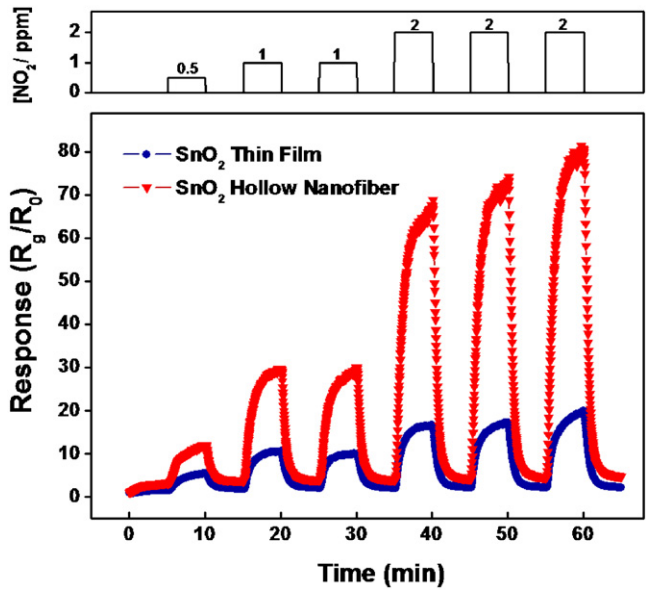

Fig. 4. Response ($S = R_{gas}/R_{air}$ to NO_2 gas at 300 °C); SnO_2 HNFs vs thin films serving as a reference.

CuK_α radiation), and β is the full width at half maximum of the diffraction peak at 2θ) as a function of the FWHM (full width at half maximum) intensity of the (1 1 0) plane of the XRD pattern. The calculated grain size comprising the SnO_2 hollow fiber was 10 nm.

To investigate the microstructure of the SnO_2 HNFs in greater detail, TEM and HR-TEM characterizations were carried out. Fig. 3a shows TEM micrographs of randomly distributed SnO_2 HNFs with diameters in the range of 300–500 nm. This image indicates that the surfaces of the HNFs are smooth and uniform and that the length of the fibers can reach tens of micrometers. As indicated in Fig. 3b, the shell thickness of the hollow SnO_2 fibers is approximately 15–20 nm, consistent with the SEM image in Fig. 1d. The inset image of Fig. 3b shows selected-area electron diffraction (SAED) patterns of a polycrystalline HNF structure with characteristic peaks of (1 1 0), (1 0 1) and (2 0 0). Fig. 3c shows an HR-TEM image of an HNF, indicating a polycrystalline SnO_2 structure with an average grain size of approximately 10 nm. This is in good agreement with the grain size (10 nm) calculated by Scherrer's equations. In Fig. 3d, a lattice image of 3.19 Å and 3.35 Å is clearly observable, corresponding to the {0 0 1} and {1 1 0} planes of the rutile (tetragonal) SnO_2 structure, respectively. The corresponding fast Fourier transform (FFT) pattern of the lattice image, i.e., the white circle, in the figure along the [1 1 0] zone axis direction, confirms the rutile SnO_2 structure (inset image in Fig. 3d).

To examine the gas sensing characteristics of the SnO_2 HFs, DC conductivity measurements were carried out in an NO_2 gas atmosphere. Fig. 4 shows the gas response (R_{gas}/R_{air}) of the SnO_2 HNFs and planar SnO_2 thin films upon exposure to successive cycles (5 min of exposure followed by 5 min of recovery in dry air) of NO_2 gas at 300 °C. The NO_2 concentration increased from 0.5 to 2 ppm, as indicated in the top part of Fig. 4. The gas response is defined as the resistance of the sensor at a given concentration of the target gas (R_{gas}) normalized by the resistance in the absence of the target gas (R_{air}). The base resistances of the SnO_2 thin films and SnO_2 HNFs were 1 kΩ and 13 kΩ, respectively. The 13-fold increase in resistance of the SnO_2 HNFs is due to their highly porous nature as well as the greater extent of electron depletion associated with the thinner walls of the fibers as compared to the films. Generally, sensor materials are sintered at relatively high temperature (>600 °C) to stabilize the microstructure and phase distribution. For *n*-type semiconducting metal oxides, this also locks in a reduced base resistance given that these oxides tend to lose oxygen upon heating leaving behind oxygen vacancy or metal interstitial donors [17,18]. However, higher temperature sintering also leads to grain growth and the consequent decrease of sensor performance [19]. For example, when the grain size exceeds about 20 nm, sensor response decreases markedly. The base resistance of 13 kΩ, achieved in SnO_2 HNFs, is moderate and readily monitored with inexpensive electronics.

The electrical resistance of the SnO_2 HNFs sensor is observed to increase with increasing concentration of NO_2 gas, an oxidizing agent. This is consistent with expectations given that chemisorbed oxidants are known to withdraw electrons from *n*-type semiconductors with the resultant formation of a zone depleted of electrons adjacent to the semiconductor/gas interface. As is well known, at a sensor operating temperature of 300 °C, the dominant species on SnO_2 surfaces is O^-, i.e. the atomic surface oxygen ion [20]. Oxidizing gases like NO_2 are known to adsorb as anions like NO_2^-, $NO_{2(gas)} + e^- = NO_2^-{}_{(ads)}$. This adsorption competes with that of oxygen, $O_{2(gas)} + 2e^- = 2O^-{}_{(ads)}$. The O^- and NO_2^- adsorbents together provide the total surface charge density. Given that adsorption of NO_2 gas is considerably stronger than that of O_2, the surface potential barrier will increase further upon exposure to the NO_2 gas, resulting in an increase in sensor resistance, even when the partial pressure of NO_2 is considerably below that of O_2.

The responsivity of the SnO_2 HNFs (R_{gas}/R_{air}) at 300 °C to 0.5, 1, and 2 ppm NO_2 was 12, 30.1, and 81.4, respectively. On the other hand, the responsivity of the planar SnO_2 thin films to 0.5, 1, and 2 ppm NO_2 was 5.5, 10.6, and 19.9, respectively, considerably lower that the HNF configuration, which displayed a 4-fold enhancement (at 2 ppm NO_2) of response compared to the non-templated planar films. In order to extract the response times (τ_{res}), the resistance curves were fitted by a simple exponential function of the form, $R(t) = a + b\exp(-t/\tau_{res})$ with *a*, *b* and *t* being fitting parameters. The τ_{res} values upon exposure to 0.5, 1, and 2 ppm NO_2 were 96, 56, and 55 s for the planar film and 79, 57, and 55 s for HNF, respectively. Improvement in gas response can be explained on the basis of the enhanced surface area of the HNF sensor, as supported by microscopy images. The unique morphological features, high surface-area-to-volume ratio and open porosity, provide larger reaction areas to the target gases. However, a more quantitative explanation for the 2–4-fold improvement in gas response requires consideration of other parameters. Obviously the hollow nanofiber has an asymmetric wall thickness varying from top to bottom [13]. The asymmetrical wall thickness arises from shadowing effects when the metal oxide film is deposited over PVP-PMMA fiber. The thinner parts of the hollow nanofibers can have relatively high resistances resulting from the formation of the depleted regions in vicinity of the potential barriers [21]. The same can occur at the contact points between nanofibers, making the resistance higher [22]. Also, SnO_2 deposits not only on the templated fibers, but also on the substrate in planar form during sputtering of the SnO_2 overlayer. Thus, a fraction of the electrons follow a conduction pathway through this planar film and bypassing the fibers. However, those parameters are difficult to extract numerically due to the highly disordered network of fibers. For a more exact and reliable characterization, extremely simple model structures (for example, a single fiber) are necessary. In subsequent studies, attempts will be made to further improve gas response by modifying the packing density of the fibers to minimize deposition directly onto the substrate, by further controlling wall thickness and introducing catalytic modification of the surfaces of the hollow tubes.

4. Conclusion

Polycrystalline SnO_2 HNFs were fabricated by depositing a SnO_2 overlayer onto electrospun PVP-PMMA nanofiber templates with subsequent calcination at 450 °C. This procedure resulted in the removal of the fiber template by thermal decomposition and the crystallization of the SnO_2 overlayers. These SnO_2 HNFs were synthesized in the form of nonwoven randomly oriented mats, which showed high surface-to-volume ratios and high porosity, allowing gases to easily penetrate into the sensing layers. Gas sensors based on the SnO_2 HNFs showed a 4-fold higher gas response (R_{gas}/R_{air}: 81.4 at 2 ppm) compared to those using SnO_2 thin films (R_{gas}/R_{air}: 19.9 at 2 ppm) in terms of their NO_2 gas detection capabilities. The higher gas response of the SnO_2 HNFs sensors is attributed to the increased surface area and enhanced carrier depletion of the thin hollow SnO_2 shells. The synthesis method described in this work is facile and versatile, providing opportunities to control the morphology of various semiconducting metal oxides with HNF structures, with particular promise for application in gas sensors.

Acknowledgements

This work was supported by a grant from the Ministry of Research, Korea and the Ministry of Science & Technology, Israel, and a grant (No. K0004114) from the Fundamental Research and Development Program for Core Technology of Materials funded by the Ministry of Knowledge Economy, Republic of Korea.

References

[1] X.J. Huang, Y.K. Choi, Chemical sensors based on nanostructured materials, Sens. Actuat. B 122 (2007) 659–671.
[2] J.G. Lu, P. Chang, Z. Fan, Quasi-one-dimensional metal oxide materials-Synthesis, properties and applications, Mater. Sci. Eng. R 52 (2006) 49–91.
[3] R.L. Vander Wal, G.W. Hunter, J.C. Xu, M.J. Kulis, G.M. Berger, T.M. Ticich, Metal-oxide nanostructure and gas-sensing performance, Sens. Actuat. B 138 (2009) 113–119.
[4] E. Comini, Metal oxide nano-crystals for gas sensing, Anal. Chim. Acta 568 (2006) 28–40.
[5] Y. Zhao, L. Jiang, Hollow micro/nanomaterials with multilevel interior structures, Adv. Mater. 21 (2009) 3621–3638.
[6] J.H. Lee, Gas sensors using hierarchical and hollow oxide nanostructures: overview, Sens. Actuat. B 140 (2009) 319–336.
[7] P.C. Chen, G. Shen, C. Zhou, Chemical sensors and electronic noses based on 1-D metal oxide nanostructures, IEEE Trans. Nanotechnol. 7 (2008) 668–682.
[8] N.S. Ramgir, Y. Yang, M. Zacharias, Nanowire-based sensors, Small 6 (2010) 1705–1722.
[9] I.D. Kim, A. Rothschild, B.H. Lee, D.Y. Kim, S.M. Jo, H.L. Tuller, Ultrasensitive chemiresistors based on electrospun TiO_2 nanofibers, Nano Lett. 6 (2006) 2009–2013.
[10] J.T. McCann, D. Li, Y. Xia, Electrospinning of nanofibers with core-sheath, hollow, or porous structures, J. Mater. Chem. 15 (2005) 735–738.
[11] V. Thavasi, G. Singh, S. Ramakrishna, Electrospun nanofibers in energy and environmental applications, Energy Environ. Sci. 1 (2008) 205–221.
[12] Y.E. Chang, D.Y. Youn, G. Ankonina, Dae. Jin Yang, H.G. Kim, A. Rothschild, I.D. Kim, Fabrication and gas sensing properties of hollow SnO_2 hemispheres, Chem. Commun. 45 (2009) 4019–4021.
[13] S.H. Choi, G. Ankonina, D.Y. Youn, S.G. Oh, J.M. Hong, A. Rothschild, I.D. Kim, Hollow ZnO nanofibers fabricated using electrospun polymer templates and their electronic transport properties, ACS Nano 3 (2009) 2623–2631.
[14] H. Wu, Y. Sun, D. Lin, R. Zhang, C. Zhang, W. Pan, GaN nanofibers based on electrospinning: facile synthesis, controlled assembly, precise doping, and application as high performance UV photodetector, Adv. Mater. 21 (2009) 227–231.
[15] J. Miao, M. Miyauchi, T.J. Simmons, J.S. Dordick, R.J. Linhardt, Electrospinning of nanomaterials and applications in electronic components and device, J. Nanosci. Nanotechnol. 10 (2010) 5507–5519.
[16] G. Wee, H.Z. Soh, Y.L. Cheah, S.G. Mhaisalkar, M. Srinivasan, Synthesis and electrochemical properties of electrospun V_2O_5 nanofibers as supercapacitor electrodes, J. Mater. Chem. 20 (2010) 6720–6725.
[17] B.M. Kulwicki, A. Amin, S.J. Lukasiewicz, S. Subramanyam, H.L. Tuller, Ceramic sensors, in: R. Buchanan (Ed.), Ceramic Materials for Electronics, 3rd edition, Marcel Dekker, New York, Basel, 2004, pp. 377–429.
[18] H.L. Tuller, S.J. Litzelman, G.C. Whitfield, Electrical conduction in nanostructured ceramics, in: R. Riedel, I.-W. Chen (Eds.), Ceramics Science and Technology Volume 2: Properties, Wiley-VCH, Weinheim, Germany, 2010, pp. 697–727.
[19] A. Rothschild, Y. Komem, The effect of grain size on the sensitivity of nanocrystalline metal-oxide gas sensors, J. Appl. Phys. 95 (2004) 6374–6380.
[20] N. Yamazoe, K. Shimanoe, Theory of power laws for semiconductor gas sensors, Sens. Actuat. B 128 (2008) 566–573.
[21] S. Dmitriev, Y. Lilach, B. Button, M. Moskovits, A. Kolmakov, Nanoengineered chemiresistors: the interplay between electron transport and chemisorption properties of morphologically encoded SnO_2 nanowires, Nanotechnology 18 (2007) 055707.
[22] V.V. Sysoev, T. Schneider, J. Goschnick, I. Kiselev, W. Habicht, H. Hahn, E. Strelcov, A. Kolmakov, Percolating SnO_2 nanowire network as a stable gas sensor: direct comparison of long-term performance versus SnO_2 nanoparticle films, Sens. Actuat. B 139 (2009) 699–703.

Biographies

Nam Gyu Cho received his Ph.D degree (2011) in materials science and engineering from Korea Advanced Institute of Science and Technology, working on inorganic hollow nanostructures using polymer templates for electrochemical devices, including metal oxide chemical gas sensors and nanostructured catalyst under the supervision of Prof. Ho-Gi Kim.

Dae Jin Yang received his PhD degree in materials science and engineering from Korea Advanced Institute of Science and Technology (2008). He was a postdoc fellow in Korea Institute of Science and Technology for 2 years. At present he is working with Prof. Harry Tuller as a postdoc at the Department of Materials Science and Engineering at MIT. His research interests are centered mainly in the fields of novel nanomaterial architectures, with particular emphasis on dye-sensitized solar cell, modified photo-electrodes and electrochemical sensors.

Mi-Jin Jin received her BS and MS in School of Advanced Materials and System Engineering at Kumoh National Institute of Technology. Her research interests include synthesis of ZnO nanowires and gas sensing characteristics of metal-oxide nanomaterials.

Ho-Gi Kim is a professor of materials science and engineering at Korea Advanced Institute of Science and Technology. He received his BS degree in ceramic engineering from the University of Hanyang (1980) and his PhD in materials engineering from Erlangen University (Germany). After a doctoral stay in Germany, he became chief of the R&D center at Firmengruppe Roederstein (1981–1983). He is currently a member of the American Ceramic Society, Integrated Ferroelectrics, chief of the Electrocomponent Materials Design Education Center, and a member of the National Association for Scientist & Engineers of Korea.

Harry L. Tuller is a member of the faculty of the Department of Materials Science and Engineering at MIT, where he serves as Professor of Ceramics and Electronic Materials and Director of the Crystal Physics and Electroceramics Laboratory. He obtained his BS and MS in Electrical Engineering and his Eng.Sc.D in Solid State Sc. & Eng at Columbia University School of Engineering. His research has emphasized the modeling, processing, characterization and optimization of energy related devices (sensors, batteries, fuel cells, solar/photolysis cells) and the integration of sensor, actuator and photonic materials into microelectromechanical (MEMS) systems. This work has been extensively published in the form of articles- 355, co-edited books-12 and patents-25. Prof. Tuller has received many honors including Docteur Honoris Causa Univ Oulu, Finland (2009) and Universite Aix-Marseille (2004); Fellow of American Ceramic Society; Fulbright-Awardee/Visiting Professor Univ. Paris; von Humboldt Fellow (Germany); and member of World Academy of Ceramics. Prof. Tuller is editor-in-chief of the Journal of Electroceramics and co-founder of Boston MicroSystems, Inc. with focus on development of MEMS-based harsh environment compatible devices to detect explosives, toxic chemicals and automotive emissions.

Il-Doo Kim received his PhD degree (2002) in Materials Science and Engineering from KAIST. From 2003 to 2005, he was a postdoctoral fellow with Prof. Harry L. Tuller at the Department of Materials Science and Engineering at MIT. In April of 2005, he returned to Korea Institute of Science and Technology as a senior research scientist. Dr. Kim's current research emphasizes processing, characterization, modeling, and optimization of solid-state devices for environmental (sensors) and energy applications (batteries and solar cells) as well as ZnO-based electronics including plastic transistors. He joined at KAIST as a faculty member in department of materials science and engineering from Feb. 2011. He has published over 78 articles and holds 60 patents. Dr. Il-Doo Kim is a member of the editorial board of the Journal of Electroceramics, Springer Academic Publishers.